NUMERICAL STUDY ON CONVECTIVE HEAT TRANSFER OF GAS-LIQUID SLUG FLOW IN A MICRO TUBE

Qunwu He, Yosuke Hasegawa and Nobuhide Kasagi

Department of Mechanical Engineering, The University of Tokyo
Hongo 7-3-1, Bunkyo-ku, Tokyo, 113-8656, Japan

ABSTRACT

Numerical simulation of gas-liquid slug flows in a micro tube is carried out. A focus is laid upon the two-phase convective heat transfer without phase change. The finite difference method is used to solve the governing equations while Phase-Field method is adopted to capture the interface. The Peclet number, Pe_T, spans a wide range from about 30 to 6000. It is found that the gas bubble works to facilitate the circulation in the liquid slug and nearly all the heat is transported by the liquid phase. When Pe_T is low, the thermal diffusion dominates the heat transfer in liquid slug while circulation is dominant at high Pe_T number. A heat transfer model is proposed to analyze and predict the heat transfer dominated by circulation. It contains three sub-regions of a gas plug, a liquid plug and a residual film. Analysis and simulation are carried out for determining the film thickness and heat transfer rate in the liquid plug. Good agreement on the global Nusselt number is confirmed between the results from model prediction and direct simulation. The resultant two-phase heat transfer rate is found notably higher than that of single-phase flow and the heat transfer performance at expense of pressure drop is also better once the liquid slug is longer than the gas bubble.

INTRODUCTION

Gas-liquid two-phase flow is a prospective way of heat transfer for compact heat exchangers. The features of extreme dominance of surface tension force and alternate passages of gas and liquid provide a novel way for heat transfer enhancement. Moreover, the flows are rather stable due to the absence of explosive boiling. The above knowledge shows a possibility to achieve a rather high heat transfer rate with only reasonable pressure drop increase. As a prerequisite, the understanding of the related flow and heat transfer characteristics are essential.

Advanced numerical simulation provides possibilities to obtain local velocity and temperature to interpret the underlying physics. However, numerical simulation of two-phase flow in a micro conduit is not a easy task due to the dominant surface tension force and the abrupt change of density. He and Kasagi [1] found that the Phase-Field method coupled with the chemical potential formulation of surface tension force can significantly suppress the parasitic flow when simulating two-phase flow at small capillary-number. This method was applied to study the pressure drop characteristics for bubbly and slug flows in a micro tube by He and Kasagi [2]. Concerning heat transfer, Oliver and Hoon [3] studied convective heat transfer of slug flows in a macro-sized tube by using viscoelastic fluids. Numerically, Fukagata et al. [4] simulated slug flows in a micro tube of 20μm ID and reported that the period of bubbles considerably affected the flow patterns and heat transfer.

Although some studies have been carried out, systematic investigations are still needed. In the present work, the numerical method proposed by He and Kasagi [1] is extended to the simulation of gas-liquid slug flows and convective heat transfer in a micro tube. Based on the obtained knowledge on heat transfer feature, a new model is developed to quantitatively predict and analyze the convective heat transfer rate. Finally, the heat transfer performance at the cost of pressure drop is evaluated.

MATHEMATICAL FORMULATION

A gas-liquid two-phase flow in a cylindrical pipe is considered. It is assumed that each phase is incompressible and phase change does not take place. The temperature is taken as a passive scalar. The gravity is neglected due to the dominance of surface tension force. The interface is captured by using the Phase-Field method [5]. The corresponding governing equations in dimensionless form are given as follows:

$$\nabla \cdot \vec{u} = 0, \tag{1}$$

$$\frac{\partial(\rho\vec{u})}{\partial t} + \vec{u}\cdot\nabla(\rho\vec{u}) = -\nabla p + \frac{1}{Re}\nabla\cdot[\eta(\nabla\vec{u}+\nabla\vec{u}^T)] - \frac{\sigma\gamma}{Cn\cdot We}C\nabla\mu, \tag{2}$$

$$\frac{\partial C}{\partial t} + \vec{u}\cdot\nabla C = \frac{1}{Pe_C}\nabla^2\mu, \qquad \mu = \Psi'(C) - Cn^2\nabla^2 C, \tag{3}$$

$$\frac{\partial(\rho C_p T)}{\partial t} + \vec{u}\cdot\nabla(\rho C_p T) = \frac{1}{Pe_T}\nabla\cdot\lambda\nabla T, \tag{4}$$

where C is the relative concentration of liquid. It takes 1 for liquid phase and 0 for gas phase, the transition from 1 to 0 represents the region of interface. μ is the dimensionless chemical potential, ε is an interface thickness parameter and $\Psi(C)$ is the bulk energy density defined as $C^2(1-C^2)/4$ [5].

Equations of (1) - (4) are satisfied in both gas and liquid phases, and the local fluid properties of ρ, η, λ and C_p are interpolated between those of gas and liquid according to the position of interface. The detailed principles of the Phase-Field method can be found in Anderson et al. [5] .

The flow is assumed to be periodic with constant gas bubble and liquid slug lengths. Therefore, only one section of the tube is simulated with a pair of a gas bubble and a liquid slug. The periodic length defines the computation domain, L_z. A pe-

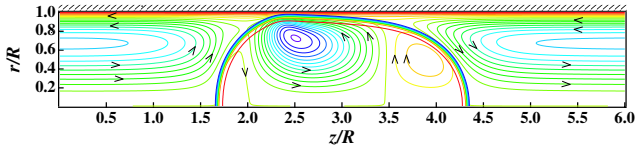

Figure 1. Bubble shape and relative streamlines, $\alpha = 0.29$ and $Re_{TP} = 288$.

riodic boundary condition is applied at the two ends of the computational domain, while conventional no-slip and fully wetted boundary conditions are used at the wall boundary. For the temperature field, a uniform heat flux, q, is assumed along the wall. Because only the temperature difference is of interest, a quasi-periodic boundary condition,

$$\left.\frac{\partial T}{\partial z}\right|_{z=0} = \left.\frac{\partial T}{\partial z}\right|_{z=L_z}, \tag{5}$$

is applied on the both ends of the computation domain.

In accordance with the experiment by Hayashi et al. [6], the water and Nitrogen at 20°C (293 K) and 1atm are employed as working fluids, and the surface tension is assumed to be 0.0728N/m. The tube diameter D is fixed at 600μm, and the characteristic velocity U_{TP}, defined as the sum of superficial liquid and gas velocities, i.e., $U_{TP} = j_G + j_L$, is given as 0.03∼1.5m/s. This range covers both bubbly and slug flows according to experimental observation [6].

RESULTS AND DISCUSSIONS

Flow Pattern

Figure 1 shows the calculated bubble shape for a representative case, where U_{TP} is used as the characteristic velocity in the definition of Re_{TP} number in accordance with experimental analysis. To visualize the induced circulation, the contours of a dimensionless stream function relative to the bubble motion, ψ, are also shown, which is defined as:

$$\frac{1}{r}\frac{\partial \psi}{\partial r} = u_z - U_{bubb}, \quad \frac{1}{r}\frac{\partial \psi}{\partial z} = -u_r. \tag{6}$$

Here, U_{bubb} is the velocity of the moving bubble. As illustrated in Fig. 1, an anti-clockwise circulation is found inside the gas phase with a relatively small clockwise circulation accompanied in the front of gas bubble. A circulation can also be found in the liquid region; it is in accordance with the sketch by Taylor [7] and visualization by Thulasidas et al. [8]. This circulation results in continuous radial movement of fluid near the gas bubble caps and thus leads to the enhancement of heat transfer.

The above simulation is repeated under different conditions of void fraction α, pressure gradient $-dp/dz$, and periodic length L_z/R. Figure 2 shows the relationship between the void fraction α and the volumetric gas flow ratio β defined as:

$$\beta = \frac{j_G}{j_G + j_L} = \alpha \frac{U_{bubb}}{U_{TP}}. \tag{7}$$

The experimental results by Hayashi et al. [6] are also shown in Fig. 2. Focusing on bubbly and slug flow regimes, he visualized

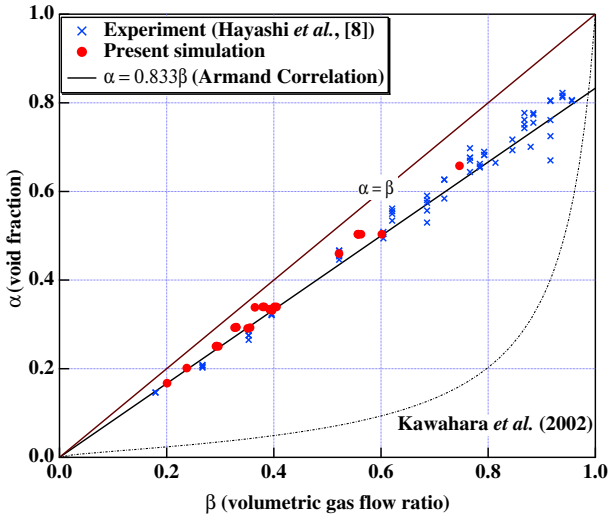

Figure 2. Relation between the volumetric gas flow ratio β and void fraction α.

the two-phase flow patterns. The relationship of α and β was calculated from the slip ratio between U_{bubb} and U_{TP}, which were obtained by measuring the gas bubble velocity with a high-speed camera and U_{TP} at the inlet, respectively.

Generally, both results of experiment and simulation lie along the so-called Armand correlation [9], which is proposed for conventional macro-sized tube as:

$$\alpha = 0.833\beta. \tag{8}$$

By combining Eqs. (7) and (8), it is straightforward to obtain:

$$\frac{U_{bubb}}{U_{TP}} = 1.2, \tag{9}$$

which implies that the bubble velocity is about 1.2 times larger than the two-phase mean velocity. The higher gas velocity corresponds to the higher centerline velocity in the tube. The scattering of both experimental and numerical results around Armand correlation is due to the different area ratios occupied by gas bubble. For a smaller area ratio, the liquid film between the gas bubble and solid wall is thicker and the gas bubble flows faster along tube center. The variation of liquid film thichness is affected by the changes of Ca number, Re number as well as gas bubble length as shown below.

Kawahara et al. [10] proposed a correlation based on the experimental data for a 100μm ID tube as:

$$\alpha = \frac{0.03\beta^{0.5}}{1 - 0.97\beta^{0.5}}, \tag{10}$$

where α is a strongly nonlinear function of β. The reported two-phase flow patterns in their study include quasi-annular and annular flows. These types of flows have relatively thicker liquid film and higher slip velocity between phases.

Temperature Distribution

Figure 3 shows the contours of dimensionless temperature at different thermal Peclet number Pe_T, where $Pe_T = Re_{TP}Pr_L$.

The dimensionless temperature, $\theta(r,z)$, is defined as:

$$\theta(r,z) = \frac{T(r,z) - \langle T_{wall} \rangle}{\langle T_{wall} \rangle - \langle T_m \rangle}, \tag{11}$$

where the bracket, $\langle \cdot \rangle$, denotes the average in the streamwise direction, $\langle T_{wall} \rangle$ and $\langle T_m \rangle$ are the domain-averaged wall and bulk mean temperatures. Accordingly, the averaged dimensionless wall temperature becomes $\langle \Theta_{wall} \rangle = 0$.

The corresponding Re_{TP} and Pr_L numbers are also shown in the figure. It is found that when $Pe_T < 200$, thermal diffusion surpasses convective heat transfer. Due to the much lower thermal capacity, the temperature in gas phase is higher than that in liquid phase. The highest temperature of the whole domain locates at the rear of gas bubble. This phenomena qualitatively agrees with the experiment observation by Monde and Mitsutake [11], who measured the wall temperature fluctuations at different streamwise positions in mini channels and reported the temperature jump corresponding to the passage of a gas bubble. Similar results have also been reported by Fukagata et al. [4]. In the liquid slug region, the bulk temperature increases along flow direction. Under this condition, the heat transfer characteristics are essentially the same as that of single-phase flow at thermally developing region.

As either Re_{TP} or Pr_L number increases, the effect of convection increases. The contours of temperature in liquid slug are consequently deformed. When $Pe_T \geq 700$, the convection dominates the heat transfer. The temperature distribution is determined by the circulation while the thermal resistance of residual film is also significant. The temperature contours in liquid slug are considered to coincide with the streamlines for $Pe_T \to \infty$. Moreover, the local fluctuation of wall temperature disappears while temperature in the residual film is obviously higher than that of liquid in circulation region and gas phase. Essentially, the two-phase flow can be deemed as that the gas bubble together with the liquid circulation region flows over the residual film and heat is transferred through the liquid film into the circulation region.

Figure 4 shows the distributions of dimensionless temperature under different liquid slug lengths L_{slug} as well as the periodic lengths L_z. In these cases the heat transfer is dominated by circulation. The distributions of dimensionless temperature are similar and the lowest temperatures are all located at the circulation center inside the liquid slug. In the regions adjacent to the bubble caps, the circulation causes radial movement of fluid between the tube center and solid wall, so that the heat transfer is enhanced. In the central region of liquid slug, the contours are nearly parallel to the axial direction. This common feature suggests a possibility of modeling the heat transfer by considering separately the heat transfer characteristics in gas bubble, liquid slug and the residual film, as discussed in the next section.

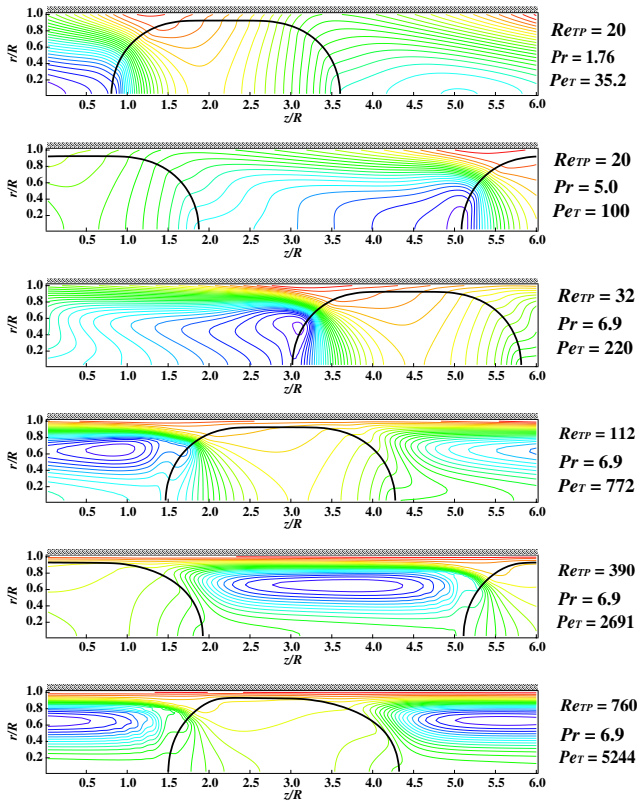

Figure 3. Contours of dimensionless temperature for different thermal Peclet number Pe_T. The red color represents for high temperature and blue for low.

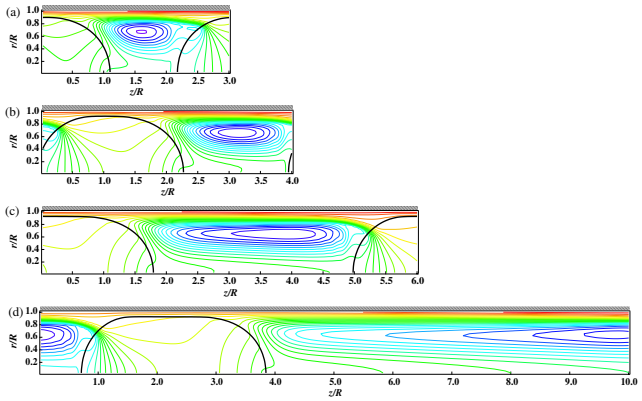

Figure 4. Distribution of dimensionless temperature for different period length L_z/R ($Re_{TP} \approx 250, Pr_L = 6.9$); (a) $L_z/R = 3$, $Nu_{slug} = 29.2$; (b) $L_z/R = 4$, $Nu_{slug} = 20.4$; (c) $L_z/R = 6$, $Nu_{slug} = 13.9$; (d) $L_z/R = 10$, $Nu_{slug} = 10.9$.

Heat Transfer

For all cases simulated in the present work, the solid wall is always wetted by liquid, i.e., the gas bubble is separated from the wall by a thin liquid film. Under this condition, the mean temperature and velocity of gas bubble are of the same order with those of liquid slug. Since the thermal capacity of the gas phase (i.e., $\rho_G C_{pG}$) is nearly 4000 times smaller than that of liquid, it is indispensable to include the fluid properties into the definition of global two-phase Nusselt number, Nu_{TP}, in order to represent the heat transfer enhancement reasonably . Therefore, the Nu_{TP} number in the present study is defined as:

$$Nu_{TP} = \frac{h_{TP} D}{\lambda_L} = \frac{2R(\partial\theta/\partial r)_{wall}}{\langle \Theta_{wall} \rangle - \langle \Theta_m \rangle} = -\frac{2R(\partial\theta/\partial r)_{wall}}{\langle \Theta_m \rangle}, \tag{12}$$

where the bulk mean temperature $\langle \Theta_m \rangle$ is defined over the whole domain as:

$$\langle \Theta_m \rangle = \frac{\int_0^{L_z} \int_0^R \rho u_z C_p \theta(r,z) dr dz}{\int_0^{L_z} \int_0^R \rho u_z C_p dr dz}. \tag{13}$$

Further, it is reasonable to assume that gas phase is nearly adiabatic and all the thermal energy imput through the wall are transferred by liquid slug. Consequently, the global Nusselt number Nu_{TP} defined by Eq. (12) can be transformed into the Nusselt number defined for the liquid slug region only by taking into account the relative length of liquid slug as:

$$Nu_{slug} = Nu_{TP}\frac{L_{bubb}+L_{slug}}{L_{slug}} = Nu_{TP}\frac{L_z}{L_{slug}}. \qquad (14)$$

The calculated Nu_{slug} numbers of four cases in Fig. 4 are shown in the caption, which change from 10.9 to 29.2 for long and short liquid slugs. With the same Pe_T numbers, this change of Nu_{slug} are due to the difference in the relative lengths of liquid slug. The effect of relative liquid slug length on the two-phase pressure drop and heat transfer rate has also been reported by several researches like He and Kasagi [2], Fukagata et al. [4] and Kreutzer et al. [12].

Heat Transfer Model

By virtues of the results shown in Fig. 4, the heat transfer of two-phase flow can be modeled by decomposing the domain into several sub-regions possessing different heat transfer mechanisms. In the present study, the focus is laid upon the cases dominated by circulation.

The present heat transfer model is schematically shown in Fig. 5. The whole domain is decomposed into three sub-regions of a gas plug, a liquid plug and the residual film between plugs and solid wall. The liquid plug region takes from the visual distance between two sequent bubbles, i.e. L_{slug}, while the gas bubble is modeled as a cylinder with radius of $r_{bubb} = R-\delta$ and length of $L_{bubb} = L_z - L_{slug}$. The residual film, also known as lubricating film in some references [12], spans beneath both the gas and liquid plugs. Theoretically, the residual film is defined as the region between wall and the dividing streamline. Moreover, it is assumed to be stable and stagnant, therefore, its thickness δ is constant. The two-phase flow is exposed to constant and uniform heat flux q at the tube wall.

It is reasonable to understand the heat transfer model shown in Fig. 5(b) as that the gas and liquid plugs alternatively flow over the residual film. At a specific position, when the gas plug appears, the thermal energy input is accumulated in the residual film due to the adiabatic property of gas phase; once the liquid arrives, the residual film is cooled by the liquid plug because of the higher thermal conductivity of liquid phase and the circulation inside the liquid plug.

Firstly, we consider the heat transfer through the residual film. Because the residual film is rather thin and adjacent to the wall, the volume flow rate through the film is negligible. Therefore, it is reasonable to assume that the mechanism of heat transfer in this region is only conduction. The corresponding thermal resistance is calculated as:

$$k_{film} = \frac{\ln(\frac{R}{R-\delta})}{2\pi\lambda_L} \qquad (15)$$

in the cylindrical coordinate. Obviously, high liquid conductivity and thin liquid film will result in small k_{film} and consequently high heat transfer rate.

Denoting the average heat transfer coefficient on the interface between the residual film and gas/liquid plugs region as $\widehat{h}_{GL}$, the

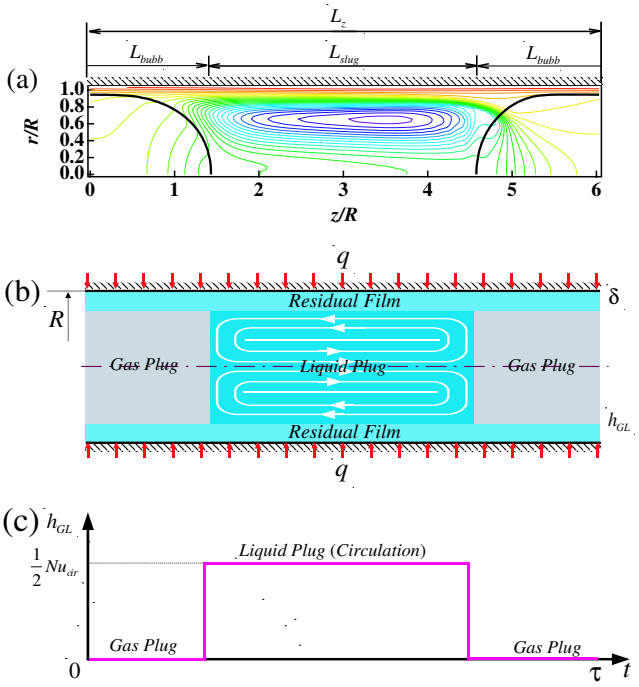

Figure 5. Heat transfer model developing. (a) Distribution of temperature; (b) Heat transfer model (not to scale); (c) Periodic boundary condition at the interface between residual film and gas/liquid plug region.

associated thermal resistance k_{GL} and mathematical definition of $\widehat{h}_{GL}$ are given as:

$$k_{GL} = \frac{1}{2\pi(R-\delta)\widehat{h}_{GL}}, \qquad \widehat{h}_{GL} = \frac{q\frac{R}{R-\delta}}{T_{GL}-T_{TP}}, \qquad (16)$$

where T_{GL} is the time-averaged temperature of the lower bottom of residual film, i.e., the interface between the residual film and gas/liquid plug region. The magnitude of $\widehat{h}_{GL}$ is mainly a function of gas and liquid plug lengths, while it is also affected by the heat transfer rate in the liquid plug as well as gas/liquid plug transport velocity.

To obtain $\widehat{h}_{GL}$, the transient heat conduction problem in the residual film has to be solved. Due to the motionlessness and uniformity of the residual film, a one-demensional conduction model is used in the present study to calculate the heat transfer in the residual film. The modeled problem is schematically illustrated in Fig. 5(b). A radial coordinate is adopted and the residual film lays along the tube wall with the thickness of δ. A constant heat flux is applied at the wall, while a heat transfer coefficient, h_{GL}, is specified at the lower bottom, which is periodic according to alternate presence of liquid and gas plugs. Because only the temperature difference is essential to determine the heat transfer coefficient, the averaged gas/liquid plug temperature is specified as $T_{TP} = 0$. The corresponding governing equation, initial and boundary conditions are given as:

$$\frac{\partial T}{\partial t} = \frac{\lambda}{\rho C_p}\frac{1}{r}\left(r\frac{\partial T}{\partial r}\right), \qquad (17)$$

$$t = 0, \qquad T(r,0) = 0, \qquad (18)$$

$$r = R, \qquad q = -\lambda\frac{\partial T(r,t)}{\partial r}\Big|_{r=R}, \qquad (19)$$

$$r = R-\delta,\ h_{GL}\left[T(R-\delta,t)-T_{TP}\right] = -\lambda\frac{\partial T(r,t)}{\partial r}\Big|_{r=R-\delta}. \qquad (20)$$

where the fluid properties, i.e., λ, ρ, and C_p are those of liquid (subscripts L are neglected for simplicity).

The convective heat transfer boundary condition at the lower boundary of residual film, h_{GL} in Eq. (20), is modeled to be a step function according to the position of gas and liquid plugs, as shown in Fig. 5(c). In the gas plug region, it is assumed to be 0 for the adiabatic gas phase assumed, while in the liquid phase region, it is the same as the mean heat transfer rate in the liquid plug and equal to $Nu_{cir}/2$ in the dimensionless form. It is apparent that the higher Nu_{cir} number and larger length ratio L_{slug}/L_{bubb} are preferred in order to obtain higher heat transfer rate.

Once the two components of thermal resistance are obtained through Eqs. (15) and (16), the global heat transfer coefficient and the corresponding Nu_{TP} are obtained as follows:

$$h_{TP} = \frac{1}{2\pi R(k_{film}+k_{GL})} = \frac{1}{\left(\frac{R\ln(\frac{R}{R-\delta})}{\lambda_L} + \frac{R}{(R-\delta)\widehat{h}_{GL}}\right)}, \quad (21)$$

$$Nu_{TP} = \frac{h_{TP}D}{\lambda_L}. \quad (22)$$

The unknown parameters are the thickness of residual film δ and the mean heat transfer rate in the liquid plug Nu_{cir}, and they will be discussed in the sequent sections, respectively.

Residual Film Thickness

A large number of experimental investigations as well as numerical simulations have been carried out to detect the thickness of residual film and associated influential parameters [12].

Bretherton [13] pioneered the use of a lubrication analysis for the transitional region where the film is formed, i.e., between the spherical front of the bubble and the flat film far behind the front. In his analysis and experiment, the inertial force was suppressed by using fluids of high viscosity. The model results in the determination of film thickness as:

$$\frac{\delta}{D} = 0.66Ca^{2/3}, \quad Ca = \frac{\eta_L U_{bubb}}{\sigma}, \quad (23)$$

where the thickness is solely dependent on the Ca number. Han and Shikazono [14] carried out systematic measurements of the liquid film thickness formed in slug flows in micro tubes of $300 \sim 1300\mu$m ID, and investigated the effects of Re number, gravity as well as gas bubble length.

The results from Eq. (23), the experiment by Han and Shikazono [14] and the present simulation are shown in Fig. 6. In simulation, the distance between the dividing streamline and solid wall at liquid slug center is taken as the residual film thickness. As shown this figure, the experimental result agrees well with Eq. (23) for long gas bubble in the region of small Ca number, while it is larger when $Ca > 0.02$ due to the effect of Re number. When the gas bubble is short, i.e., $L_{bubb}/R < 6$, the results show significant deviations, and this feature is in agreement with the simulation. The possible reason is due to the interactions between the transition regions of front and rear caps of the gas bubble.

Suo and Griffith [15] proposed a simple method to estimate the film thickness for two-phase flows dominated by surface tension force. As shown in Fig. 7, if we assume that G_{slug}, G_{bubb}

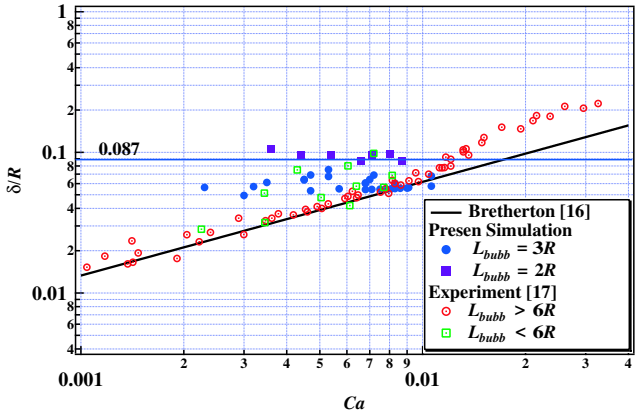

Figure 6. Thickness of residual film.

and G_{film} are the volumetric flux at the liquid slug, gas bubble and through liquid film, respectively, and they are defined as:

$$G_{slug} = \pi R^2 U_{TP}, \quad G_{bubb} = \pi r_{bubb}^2 U_{bubb}, \quad (24)$$

where r_{bubb} is radius of gas bubble, i.e., $r_{bubb} = R - \delta$.

Due to the incompressibility of both phases, the volumetric flux at each section of the tube is the same, therefore,

$$G_{slug} = G_{bubb} + G_{film}. \quad (25)$$

If we ignore the gravitational effects, the flow is axisymmetric when the surface tension is strong. According to Laplace-Young equation,

$$p_{bubb} - p_{film} = \frac{\sigma}{r_{bubb}}, \quad (26)$$

where p_{bubb} and p_{film} are the pressure in the gas bubble and liquid film, respectively. The pressure of p_{bubb} is nearly uniform due to the rather small viscosity of gas phase, so that any changes in p_{film} can only be brought about by change in r_{bubb}. For two-phase flow in micro tubes, the surface tension force is dominant, and the variations in r_{bubb} is negligible. Consequently, p_{film} is constant and $Q_{film} \approx 0$. This also means that the thickness of residual film is determined at the nose of the bubble and independent of the gas bubble length.

Assuming that m is the fraction of the cross-section area of a tube occupied by a gas bubble, we get

$$m = \frac{\pi r_{bubb}^2}{\pi R^2} = \left(\frac{r_{bubb}}{R}\right)^2 = \left(1 - \frac{\delta}{R}\right)^2. \quad (27)$$

Equations (25) and (27) become

$$R^2 U_{TP} = mR^2 U_{bubb}. \quad (28)$$

From Eqs. (7), (27) and (28), the relation between the residual film thickness, velocity ratio and the relationship of α and β are written as:

$$\left(1 - \frac{\delta}{R}\right)^2 = \frac{U_{TP}}{U_{bubb}} = \frac{\alpha}{\beta}. \quad (29)$$

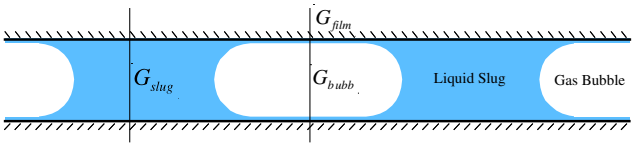

Figure 7. Volumetric flux in liquid slug and gas bubble inside a micro tube.

When the thickness δ approaching 0, the two phases will flow at the same velocity with $\alpha = \beta$. On the other limit, when $\delta \to R$, the gas bubble flows much faster than liquid and $\alpha \ll \beta$; under this condition, the circulation disappears and flow pattern also changes into annular or quasi-annular flow.

As shown in Fig. 2, we have a general relationship of $\alpha = 0.833\beta$. Substituting this relation into Eq. (29), it is straightforward to get:

$$\frac{r_{bubb}}{R} = 0.913, \qquad \frac{\delta}{R} = 0.087, \tag{30}$$

which is the value used for δ in Eq. (21) in the present study as the first-order approximation. Note that the results by Eq. (30) is an empirically averaged value which covers wide ranges of *Ca* number, *Re* number as well as lengths of liquid slug and gas bubble. The procedure above also provides an indirect way to estimate the residual film thickness from the bubble velocity and flow rates; this is much easier than the direct measurement as done by Han and Shikazono [14].

Flow and Heat Transfer in Liquid Plug

As shown in Fig. 4, the heat transfer in liquid plug is affected by *Re* number, *Pr* number as well as the liquid slug length. To find a relationship of

$$Nu_{cir} = f(Re_{TP}, Pr_L, L_{slug}), \tag{31}$$

which is used to calculate h_{GL} in Eq. (20), a series of simulation has been carried out. The simulation model is illustrated in Fig. 8, where the gas phase is assumed to contact the wall directly and the contact angle is set to be 90 degrees in accordance with the modeled gas bubble configuration shown in Fig. 5(b). By using this model it is confirmed that the effect of residual film is eliminated and the heat transfer characteristics in liquid plug can be studied separately. The singularity at the contact point in simulation is resolved by diffusion which is driven by chemical potential gradient [16]. The fluid properties are the same as those stated above while the *Pr* number is changed from 1.67 to 6.96 corresponding to the water at 100^{o}C and 20^{o}C, respectively.

Figure 8 shows distribution of the relative streamlines for different Re_{TP} numbers of 106, 482 and 719. Despite the significant change of Re_{TP} number, the distributions of streamlines are almost the same. In addition, the streamlines as well as the location of circulation center are nearly identical to the analytical results by Duda and Vrentas [17], who studied the same problem in the limit of $Re_{TP} \to 0$. It is apparent that, except the interface deformation, the effect of Re_{TP} number on the flow field in the liquid plug is negligible. Consequently, the Re_{TP} and Pr_L numbers have the same power index in Eq. (31), i.e., $Nu_{cir} = f(Re_{TP}Pr_L, L_{slug}) = f(Pe_T, L_{slug})$.

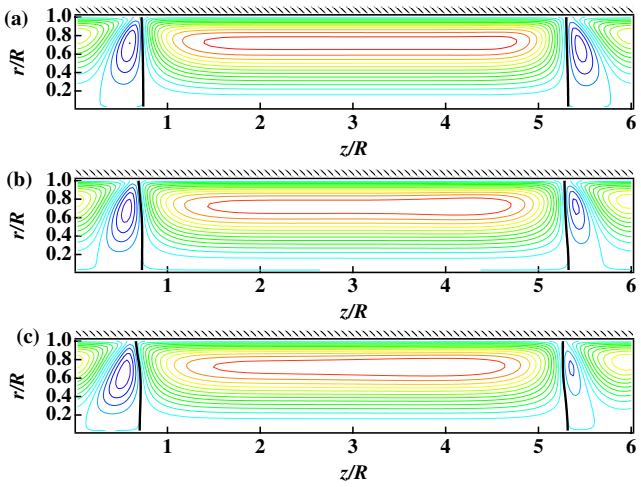

Figure 8. Relative streamlines for different Re_{TP} numbers. (a) $Re_{TP} = 106$; (b) $Re_{TP} = 482$; (c) $Re_{TP} = 719$.

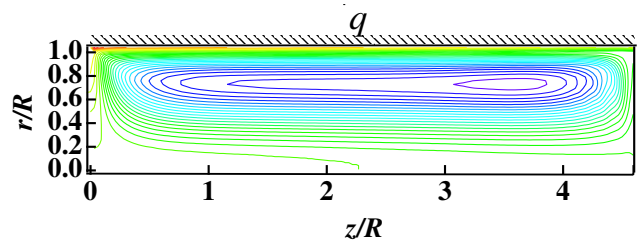

Figure 9. Contours of temperature in the liquid plug. ($L_{cir}/R = 4.6, Re_{TP} = 736, Pe_T = 5078$)

In accordance with the heat transfer model, the heat transfer in liquid plug is studied here. A constant heat flux is applied at the solid wall in the liquid phase region and the gas phase is assumed to be adiabatic. The temperature distribution in a typical case is shown in Fig. 9. The contours of temperature possess essentially the same characteristics as those shown in Fig. 4 and circulation dominates the heat transfer.

The simulation is repeated under different conditions of Re_{TP} number and liquid plug length L_{cir}, i.e., $Re_{TP} = 30 \sim 900, Pe_T = Re_{TP}Pr_L = 200 \sim 6300$ and $L_{cir}/R = 1 \sim 8.6$. The calculated Nu_{cir} is correlated by fitting, and the resultant correlation is expressed as:

$$Nu_{cir} = 24.2 + 0.54 Pe_T^{0.45} (L_{cir}/D)^{-1.34}, \tag{32}$$

where the constant of 24.2 corresponds to the heat transfer enhancement at liquid plug center, which is almost independent on Pe_T number, while the second right-hand-side term represents the heat transfer due to the radial heat transfer at two ends of the liquid plug. In order to get larger Nu_{cir} in terms of heat transfer enhancement, high Re_{TP} and Pr_L numbers as well as short liquid slug are preferred. By considering the different power indexes of Pe_T number and L_{cir}/R, the effect of liquid slug length is more significant.

Results from Modeling

Once the averaged residual film thickness δ and the global heat transfer in the liquid plug Nu_{cir} are obtained from Eqs. (30)

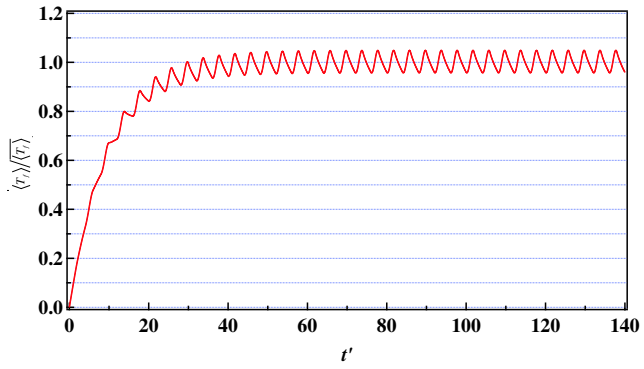

Figure 10. Variation of average temperature of the residual film.

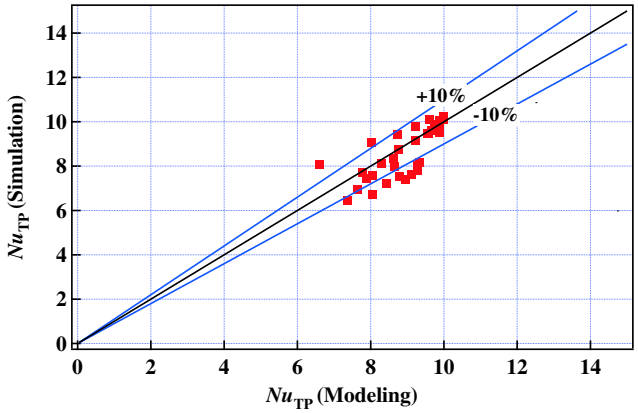

Figure 11. Comparison of Nu_{TP} for simulation and modeling.

and (32), respectively, Eqs. (17) - (20) are solved by conventional finite difference method. Figure 10 shows the fluctuation of domain-averaged temperature in the residual film. The temperature increases from the initial value and fluctuates according to the alternate passing of gas and liquid plugs.

From the transient temperature field in the residual film, $\widehat{h}_{GL}$ is calculated by Eq. (16), which is further substituted into Eq. (21). The calculated Nu_{TP} from the model described above and the results from direct numerical simulation are compared in Fig. 11. Good agreement is confirmed with an overall deviation of about $\pm 10\%$. These deviations are mainly caused by the discrepancy on the the values of heat transfer rate between liquid slug in simulation and modeled liquid plug. The resultant Nu_{TP} numbers are about $7\sim 10$, which is significantly larger than the value of 4.36 for the heat transfer by single-phase flow.

Taking a typical case as an example, i.e., $Pe_T = Re_{TP}Pr_L = 300\times 6.96 = 2088$, $L_{bubb}/R = L_{slug}/R = 3$ and $\delta/R = 0.087$, the resultant ratio of k_{film} to the overall thermal resistance is given as:

$$\frac{k_{film}}{k_{film}+k_{GL}} = 0.38. \tag{33}$$

Eq. (33) shows that the thermal resistance from the residual film and gas/liquid plug region are on the same order, while the latter is more significant. On the hand, according to the heat transfer model shown in Fig. 5 and Eq. (21), the global two-phase heat transfer rate are affected by δ, L_{bubb}, L_{slug} as well as Pe_T(i.e.,$Re_{TP}Pr_L$). To achieve a high heat transfer rate, short gas bubble and liquid slug, strong surface tension and high two-phase velocity are preferred.

To fairly evaluate the heat transfer performance, the increase of pressure drop due to the introduction of gas bubbles should also be taken into account. In the present study, the phenomenological model for predicting pressure drop of two-phase flow proposed by He and Kasagi [2] is adopted. Fig. 12 shows the heat transfer enhancement as the expense of pressure drop, $(Nu_{TP}/Nu_{LO})/\Phi_L^2$. Here, $Nu_{LO} = 4.36$ and Φ_L^2 is the two-phase multiplier defined as:

$$\Phi_L^2 = \frac{(-dP/dz)_{TP}}{(-dP/dz)_{LO}}. \tag{34}$$

$(-dP/dz)_{LO}$ represents the pressure gradients required to drive a single-phase liquid flow at the same superficial velocity. As shown in the figure, once $L_{slug} > L_{bubb}$, the factor exceeds unity. For longer liquid slug, the heat transfer performance is better.

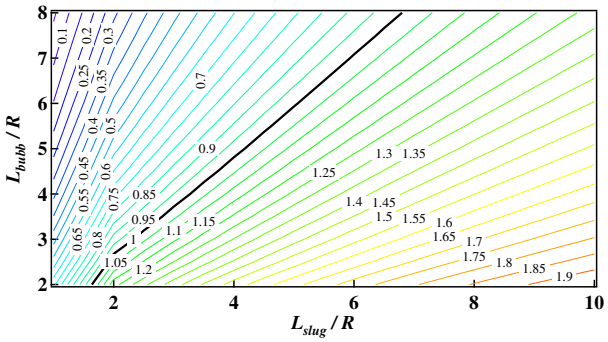

Figure 12. Heat transfer enhancement at the expense of pressure drop, $(Nu_{TP}/Nu_{LO})/\Phi_L^2$ ($Re_{TP} = 400$).

CONCLUSIONS

A series numerical simulation of Nitrogen-water two-phase slug flow in a micro tube is carried out. The computed relationship between the void fraction α and the volumetric gas flow ratio β is in agreement with the experimental results and follows the so-called Armand correction.

It is found that the gas bubble works to facilitate the circulation in the liquid slug, and the heat transported by the gas bubble is negligible. In the case of low Pe_T number, thermal diffusion dominates the heat transport in the liquid slug, which has the same characteristics with single-phase liquid flow in the thermally developing region. When the Pe_T number is large, circulation determines the heat transfer performance.

Based on the observation of temperature distributions, a new model is proposed for two-phase convective heat transfer dominated by circulation. The two-phase flow domain is decomposed into three sub-regions as an adiabatic gas plug, a liquid plug dominated by circulation and a residual film. Analyses and simulates are carried out to obtain the residual film thickness and the global heat transfer rate in the liquid plug. Good agreement in the global two-phase Nusselt number between the modeling prediction and direct simulation is confirmed. The resultant two-phase heat transfer rate is about two times that of single-phase flow and the heat transfer performance is also better if the liquid slug is longer than the gas bubble. On the other hand, once circulation is generated in the liquid slug, large Pe_T number, short gas bubble and liquid slug are recommended for obtaining higher heat transfer rate.

ACKNOWLEDGMENT

The authors are grateful to Professors Y. Suzuki and N. Shikazono for their fruitful discussions, and also Mr. H. Utashiro for his experimental measurement.

NOMENCLATURE

C concentration
Cn Cahn number, ε/D
C_p thermal capacity, [J/kg K]
Ca Capillary number, $\eta_L U/\sigma$
D tube diameter, [m]
G volumetric flux, [m^2/s]
h heat transfer coefficient, [W/K m^2]
j superficial velocity, [m/s]
k thermal resistance, [m^2 K/W]
L longitudinal length, [m]
m area ratio occupied by gas bubble to the tube cross-section
$\mathcal{M}$ dimensionless mobility
Nu Nusselt number
p pressure, [Pa]
Pe_C concentration Peclet number, $UD/(\mathcal{M}\mu_L)$
Pe_T thermal Peclet number, $\rho_L U C_{pL} D/\lambda_L$
Pr Prandtl number
q heat flux, [W/m^2]
r radial direction, [m]
R tube radius, [m]
Re Reynolds number, $\rho_L UD/\eta_L$
t time, [s]
T temperature, [K]
$\vec{u}$ velocity
We Weber number, $\rho_L U^2 D/\sigma$
U mean velocity, [m/s]
z longitudinal direction, [m]

Greek Symbols
α void fraction
β volumetric gas flow ratio
δ residual film thickness, [m]
ε interface thickness parameter
σ surface tension coefficient, [N/m]
η viscosity, [Pa s]
γ constant
μ dimensionless chemical potential
λ thermal conductivity, [W/m K]
Φ_L^2 two-phase multiplier
Ψ dimensionless bulk free energy
ψ dimensionless stream function
ρ density, [kg/m^3]
θ dimensionless temperature
Θ dimensionless mean temperature

Subscripts
bubb gas bubble
cir circulation
film residual film
G gas phase
GL gas/liquid plug region
L liquid phase
LO liquid-only
m bulk mean
slug liquid slug
TP two-phase
wall wall
z longitudinal

REFERENCES

[1] Q. He and N. Kasagi, Phase-Field simulation of small capillary-number two-phase flow in a microtube, *Fluid Dyn. Res.*, vol. 40, pp. 497–509, 2008.
[2] Q. He and N. Kasagi, Numerical investigation on flow pattern and pressure drop characteristics of slug flow in a micro tube, *Proc. 6th Int. Conf. Nanochannel, Microchannel and Minichannel*, Jun. 23-25, Darmstadt, Germany, 2008.
[3] D.R. Oliver and Y.A. Hoon, Two-phase non-newtonian flow, *Trans. Inst. Chem. Eng.*, vol. 46, pp. 116–122, 1968.
[4] K. Fukagata, N. Kasagi, P. Ua-arayaporn and T. Himeno, Numerical simulation of gas-liquid two-phase flow and convective heat transfer in a micro tube, *Int. J. Heat Fluid Flow*, vol. 27, pp. 72–82, 2007.
[5] D.M. Anderson, G.B. McFadden and A.A. Wheeler, Diffuse-interface methods in fluids mechanics, *Annu. Rev. Fluid Mech.*, vol. 30, pp.139–165, 1998.
[6] S. Hayashi, N. Kasagi, and Y. Suzuki, The effects of inlet flow conditions on gas-liquid two-phase flow in a micro tube, *Proc. HT2007 & 2007 ASME-JSME Thermal Engineering Summer Heat Transfer Conference*, Paper No. HT2007-32916, July 8-12, 2007, Vancouver, Canada.
[7] G.I. Taylor, Deposition of a viscous fluid on the wall of a tube, *J. Fluid Mech.*, vol. 10, pp. 1161–1165, 1961.
[8] T.C. Thulasidas, M.A. Abraham and R.L. Cerro, Flow patterns in liquid slugs during bubble-train flow inside capillaries, *Chem. Eng. Sci.*, vol. 52, pp. 2947–2962, 1997.
[9] A.A. Armand and G.G. Treschev, The resistance during the movement of a two-phase systems in horizontal pipe. *Izv, Vses, Teplotek. Inst.*, vol. 1, pp. 16-23, 1946.
[10] A. Kawahara, P.M.-Y Chung, and M. Kawaji, Investigation of two-phase flow pattern, void fraction and pressure drop in a microchannel. *Int. J. Multiphase Flow*, vol. 28, pp. 1411–1435, 2002.
[11] M. Monde, and Y. Mitsutake, Enhancement of heat transfer due to bubbles passing through a narrow vertical rectangular channel (Change in heat transfer along flow), *Heat Mass Transfer*, vol. 31, pp. 77–82, 1995.
[12] M.T. Kreutzer, F. Kapteijn, J.A. Moulijn and J.J. Heiszwolf, Multiphase monolith reactors: Chemical reaction engineering of segmented flow in microchannels, *Chem. Eng. Sci*, vol. 60, pp. 5895–5916, 2005.
[13] F.P. Bretherton, The motion of long bubbles in tubes. *J. Fluid Mech.*, vol. 10, pp.166–188, 1961.
[14] Y.B. Han and N. Shikazono, Thickness of liquid film formed in slug flow in micro tube. *Proc. ECI Conf. on Heat Transfer and Fluid Flow in Microscale*, Hilton Whistler, Canada, Sep. 21-26, 2008.
[15] M. Suo and P. Griffith, Two-phase flow in capillary tubes, *J. Basic Eng. ASME*, vol. 86, pp. 576–582, 1964.
[16] D. Jacqmin, Contact-line dynamics of a diffuse fluid interface, *J. Fluid. Mech.*, vol. 402, pp. 57–88, 2000.
[17] J.L. Duda and J.S. Vrentas, Steady flow in the region of closed streamlines in a cylindrical cavity. *J. Fluid Mech.*, vol. 45, pp. 247-260, 1971.